Chapter 8
Fermentative Alcohol Production

Mariano Martín, Antonio Sánchez and John M. Woodley

Nomenclature

a	Specific area (m^{-1})
a′	Horizontal diameter of the bubble (m)
A	Contact area (m^2)
A_r	Instantaneous area of the bubble (m^2)
A_{ref}	Bubble surface area as a rigid body (m^2)
b′	Vertical diameter of the bubble (m)
b	Bubble cup half height (m)
c	Concentration (mol L^{-1})
c_A	Concentration of species A (mol L^{-1})
C	Bubble cup half length (m)
C*	Saturation concentration (kg m^{-3})
C_D	Drag coefficient
C_i	Constants
D_i	Diffusion coefficient of component i (m^2 s^{-1})
d_{32}	Sauter meandiameter (m)
d_b	Initial bubble diameter (m)
d_{eq}	Equivalent bubble diameter (m)
d_{max}	Maximum stable bubble diameter (m)
D_{AB}	Molecular diffusivity of A in B (m^2 s^{-1})
eff	Fouling coefficients
E	2C/2b as defined in Fig. 7
Et	Ethanol concentration (g dm^{-3})
*Et**	Saturation concentration of ethanol (g dm^{-3})
Fl_G	Aeration number $Fl_G = \frac{Q_c}{NT^3}$

M. Martín (✉) · A. Sánchez
Departamento de Ingeniería Química y textil, University of Salamanca,
Plz. Caídos 1–5, 37008 Salamanca, Spain
e-mail: mariano.m3@usal.es

J. M. Woodley
Department of Chemical and Biochemical Engineering, Technical University of Denmark,
Søltofts Plads 229 2800 Kgs. Lyngby, Copenhagen, Denmark

Q. Liao et al. (eds.), *Bioreactors for Microbial Biomass and Energy Conversion*,
Green Energy and Technology, https://doi.org/10.1007/978-981-10-7677-0_8

Fr Froude number $\mathrm{Fr} = \frac{\mathrm{TN}^2}{\mathrm{g}}$

g Gravity constant, 9.8 m s^{-2}

G Glucose concentration (g dm^{-3})

Gr Grashof number $\mathrm{Gr} = \frac{\mathrm{d}_\mathrm{b}^3 \rho \cdot \Delta\rho \cdot g}{\mu \cdot \mathrm{D}_{\mathrm{AB}}}$

h_i Film resistance inside the vessel (J m^{-2} K^{-1})

h_e Film resistance of the fluid (J m^{-2} K^{-1})

k Film resistance of the jacket (J m^{-2} K^{-1})

k_L Liquid film resistance (m s^{-1})

$k_{H,i}$ Henry coefficient of component I (mol l^{-1} atm^{-1})

K_s Substrate concentration corresponding to 1/2 μ_{max} (g dm^{-3})

K_I Inhibition equilibrium constant (mol l^{-1})

K_{mj} Concentration of the metabolite, where the rate is equal to half of Vmax and j is the number of corresponding reactions (mM)

K_{isj} Inhibition constant for the substrate, where j is number of corresponding reactions (mM)

K_{iij} Inhibition constant for the inhibitor, where j is the number of corresponding reactions (mM)

K_{aj} Activation constant for the activator, where j is the number of corresponding reactions (mM)

k_G Gas phase resistance to mass transfer (m s^{-1})

K Global phase resistance to mass transfer (m s^{-1})

k_i Interphase resistance to mass transfer (m s^{-1})

k_La Volumetric mass transfer coefficient (s^{-1})

k_f Conductivity (J s^{-1} m^{-1} K^{-1})

K_s The half velocity constant (M)

m Maintenance utilization (h^{-1})

N_i Molar flux (mol m^{-2} s^{-1})

N Impeller speed (s^{-1})

Nu Nusselt number $\mathrm{N}u = \frac{\mathrm{h} \cdot \mathrm{L}}{\mathrm{k}_\mathrm{f}}$

P Product (Ethanol) concentration (g dm^{-3})

P Impeller power (W)

P_g Aerated power (W)

P_o Power number $\mathrm{P_o} = \frac{\mathrm{P}}{\mathrm{T}^5 \mathrm{N}^3 \rho}$

P_m Ethanol concentration above which cells do not grow (g dm^{-3})

P'_m Ethanol concentration above which cells do not produce ethanol (g dm^{-3})

Pe Peclet number $\mathrm{Pe} = \frac{\mathrm{U_B} \cdot \mathrm{d_b}}{\mathrm{D_{AB}}}$

Pr Prandtl number $\mathrm{Pr} = \frac{\mathrm{Cp} \cdot \mu}{\mathrm{k}}$

Q_c Gas flow rate (m^3 s^{-1})

Q Pumping capacity (Eq. 1)

q Specific rate of substrate utilization (g dm^{-3} h^{-1})

q_{max} Maximum specific rate of substrate utilization (g dm^{-3} h^{-1})

R	Bubble radius (m)
R_g	Constant of the gases (Pa m^3 mol^{-1} K^{-1})
RPD	Gasification factor P_g/P
r_S	Overall reaction rate(mol l^{-1} s^{-1})
r_g	Rate of cell growth (g dm^{-3} h^{-1})
r_d	Rate of cell death (g dm^{-3} h^{-1})
r_{sm}	Rate of substrate consumption for maintenance (g dm^{-3} h^{-1})
Re	Reynolds number $\mathrm{Re} = \frac{T^2 N \rho}{\mu}$
S	Substrate concentration (g dm^{-3})
s	Element replacement rate (s^{-1})
Sc	Schmidt number $\mathrm{Sc} = \frac{\mu}{\rho \cdot D_{AB}}$
Sh	Sherwood number $\mathrm{Sh} = \frac{k_L d_b}{D_{AB}}$
t	Time (s)
T	Impeller diameter (m)
T_i	Impeller blades width (m)
T	Temperature (K)
U	Global heat transfer coefficient (J m^{-2} K^{-1})
U_B	Terminal rising velocity of the bubbles (m s^{-1})
V_{max}	Maximum reaction velocity (mol l^{-1} s^{-1})
V	Volume (dm^3)
x	Width of the wall (m)
X	Biomass concentration or xylose concentration (g dm^{-3})
Y_i	Yield coefficient
$Y_{X/S}$	Biomass yield from substrate
$Y_{Et/X}$	Ethanol yield from biomass
u_G	Superficial gas velocity (m s^{-1})
V	Liquid volume (m^3)
w	Blade speed (m s^{-1})
We	Weber number $\mathrm{We} = \frac{\rho N^2 T^3}{\sigma}$
x_A	Molar fraction of species A
z	Vertical coordinate (m)
z_b	Film thickness (m)

Greek Symbols

α, β, α′, β′, α″, β″ and δ	Empirical coefficients
α	Fraction of molecules hitting the surface
α_i	Fraction of the bubble surface
β_i	Mass transfer coefficient (m s^{-1})
β, δ	Empirical coefficients
β	Inhibition constant
δ_o	Boundary layer thickness (m)

ε	Dissipated energy (W kg^{-1})
ε_G	Gas hold up
ρ	Liquid density (kg m^{-3})
ρ_G	Gas density (kg m^{-3})
ρ_i	Reaction rate of component i (mol l^{-1} h^{-1})
μ	Liquid viscosity (Pa s)
σ	Surface tension (N m^{-1})
ε_G	Gas hold up
η	Turbulence characteristic length (m)
ν	Kinematic liquid viscosity (m^2 s^{-1})
γ	Stress (N m^{-2})
μ_{max}	Maximum specific growth rate of the biomass (h^{-1})
μ	Specific growth rate of the biomass (g dm^{-3} h^{-1})
μ_w	Water viscosity (Pa s)
γ	Inhibition constant
υ_i	Specific productivities of component i

1 Introduction

Bioethanol production is typically focused on the use of sugar to obtain ethanol via anaerobic fermentation. This has been the main path used by most first and second generation bioethanol plants all over the world. However, this particular case only covers one example of units and mechanisms for the production of alcohols intended as fuels. A broader view of the problem presents two different feedstocks, not only sugar but also syngas. The principles for the fermentation of both resources are similar, although, while sugar fermentation is a single phase reaction, liquid, where a solution of water and ethanol is produced in jacketed stirred tank reactors, the use of syngas expands the complexity into gas-liquid type bioreactors. These two phase reactors are governed by the mass transfer between the gas, the raw materials, and the liquid, where the ethanol will be obtained. This fact provides a further degree of freedom in terms of reactor design, not only stirred tanks but also bubble columns can be used. This alternative has its supporters but it has not been fully deployed. Furthermore, ethanol is not the only fermentative alcohol of choice as a biofuel, and lately, biobutanol has gained particular interest. In order to cover the basics for the design of the units used for such processes, we have divided this chapter into the principles and the applications. Section 2 presents the hydrodynamics of the units as well as mass transfer rate limitations in the case of gas-liquid systems; the energy transfer required to cool an exothermic reaction and the kinetic mechanisms. Section 3 presents examples for bioethanol and biobutanol production. The kinetics of the production of alcohols from syngas or glucose is based on the Monod model that evaluates the growth of microorganisms such as *Sacharomices cerevisiae, Zymonas Mobilis*, etc. While the basic model is quite

simple, the fact that alcohols inhibit that growth requires the addition of terms to account for that inhibition in the models.

2 Reactor Design Principles

This section is divided into single phase reactors (ignoring the presence of solids), and gas-liquid reactors for application in the fermentation of sugars and syngas, respectively. This classification allows presentation of the main features of the design of such units from the hydrodynamic, as well as mass/heat transfer perspective considering the dispersion of syngas in the fermentation broth.

2.1 Liquid Systems

Within this subsection the units devoted to the fermentation of sugars are presented. This is the base case for aerated stirred tanks that will be presented in Sect. 2.2. We consider the internal hydrodynamics as well as the power input responsible for the fluid circulation in the tanks. We follow this with a discussion about heat removal. Aerobic fermentations are exothermic, and since they operate at near ambient temperature, 32–38 °C, this makes heat transfer an important challenge to be addressed.

2.1.1 Hydrodynamics

The internal flow pattern in a stirred tank is generated by the geometry, the baffles and the impeller (or agitator) used. While the geometry is often standard, and the baffles follow certain rules-of-thumb in terms of allocation and size [1], there are a number of impellers available such as Rushton turbines, pitched blade turbines, propellers and anchors. The typical classification considers those which generate an axial flow (e.g. pitched turbines), and those which generate a radial flow (e.g., Rushton turbines). Figure 1 shows the geometry of a number of commercial impellers typically used in industry [2].

Mixing within the tanks consists of bringing into contact high velocity streams inside the tank with stagnant regions of fluid so that stresses are generated on the contact surface. This mechanism develops turbulent eddies that will be incorporated in the general flow. High turbulent velocity is required for an effective mixing operation. The stream generated by the impeller must generate enough liquid flow in order to move the whole bulk liquid, while at the same time generate kinetic energy to balance the shear stress, and enough velocity so that dead volumes are minimized. Thus, the quality of mixing in a tank can be quantified using two parameters—the mixing time and the pumping capacity. The mixing time refers to

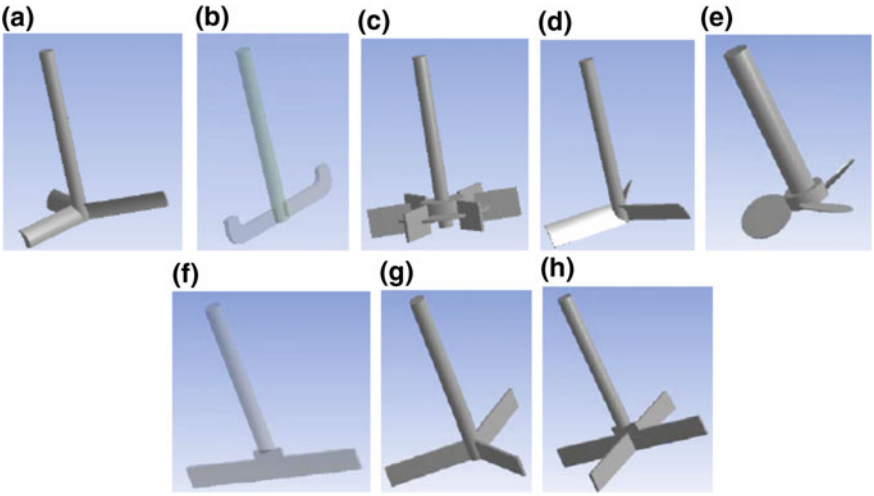

Fig. 1 Impellers geometry **a** pitched curved blade turbine; **b** anchor type turbine; **c** Rushton turbine; **d** pitched curved blade turbine; **e** propeller; **f** two bladed turbine; **g** three bladed turbine; **h** four blade turbine

the time it takes to reach 90–95% of homogeneous concentration in a tank [3]. It is proportional to the circulation time in the tank given by the liquid volume divided by the flow velocity, which is proportional to $N{\cdot}T^3$, where N is the impeller speed and T its diameter. As a result, according to Gogate et al., the mixing time is inversely proportional to the impeller speed [4]. With respect to the pumping capacity, it is assumed that the impeller behaves as a pump that moves the fluid across the tank. Equation (1) shows the expression for pumping capacity [5]:

$$Q = N_Q \cdot N \cdot T^3 \tag{1}$$

where N_Q is the dimensionless discharge coefficient.

Since the impeller acts as a pump, the power provided can be computed from an analysis of the forces acting on the impeller blades as it rotates inside a liquid with a relative velocity w [6]. The dynamic pressure exerted on the blade can be written as $\frac{1}{2}\rho w^2$, while the theoretical force is obtained by multiplying this pressure by the blade area, A. So, the theoretical force is written as $F_t = \frac{1}{2}\rho w^2 A$. The actual force on the blade is related to the theoretical force by a drag coefficient $C_{D,}$ so that the force becomes:

$$F_a = \frac{1}{2}\rho w^2 A C_D \tag{2}$$

A definition of power is obtained multiplying force by velocity, therefore giving an expression for power:

$$P = C_D \frac{1}{2} \rho w^3 A \tag{3}$$

For a paddle agitator, the frontal area A is a combination of the length of the blade and its width. Both are functions of the impeller diameter, T; thus $A \propto T^2$. Since velocity is a function of impeller diameter and speed of rotation, then $w \propto NT$. Combining these relations gives the following description of power:

$$P \propto N^3 T^5 \tag{4}$$

An experimentally proved law derived from dimensional analysis, called the "propeller law", states that the theoretical power requirement of the agitator is given by:

$$P = \rho N^3 T^5 \tag{5}$$

And the actual power, P, transmitted by the agitator is related to Eq. (5) through a coefficient, P_o.

$$P = P_o \rho N^3 T^5 \tag{6}$$

Typically P_o is termed the Power Number. The power consumed in a tank is usually calculated from the torque needed to move the fluid inside. In this way, the power transmitted by an agitator given by Eq. (6) can be related to the applied torque, M_r , [6], as follows:

$$P = 2\pi N M_r = P_o \rho N^3 T^5 \tag{7}$$

However, by means of dimensional analysis it has been proved that the power an impeller provides depends on the geometrical characteristics of the system as well as on dimensionless numbers like the Power Number, the Reynolds Number and the Froude Number (Fig. 2).

The Power Number, defined by Eq. (6), accounts for the friction forces, so it is a measure of the resistance of the liquid to move. It is proportional to the ratio between the resistance force acting on the area of the blade and the inertial force. The inertial force is related to the momentum transfer due to the global movement of the fluid. For baffled reactors, the Power Number is constant. Although from Eq. (5) it could be inferred that the number of blades should increase the power proportionately, the wake influence of upstream blades is similar to a sheltering effect and consequently the power only increases in proportion to the number of blades raised to a power in the range of 0.5–0.8. Thus, if more blades are added, the blades are subject to a diminishing local normal velocity.

The Froude Number ($Fr = \frac{TN^2}{g}$), where T is impeller diameter, g is gravity and N the revolutions per minute accounts for the relationship between the inertial force

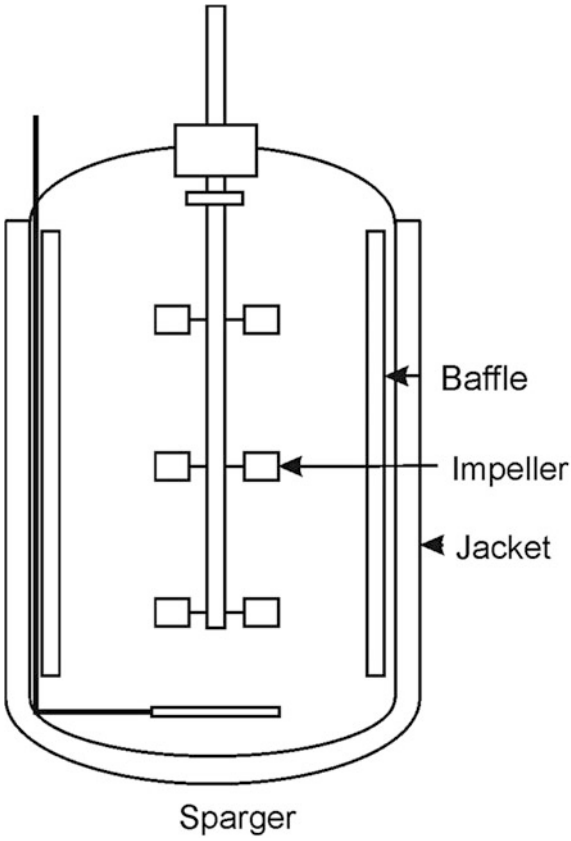

Fig. 2 Scheme for a jacketed stirred tank reactor

and the gravity per unit area acting on the fluid. It has an important effect when waves are developed on the liquid surface in the form of vortices.

The Reynolds Number ($Re = \frac{T^2 N \rho}{\mu}$), where ρ and μ are fluid density and viscosity, respectively, represents the ratio between the kinetic forces and the resistance forces. It also describes the flow regime in the tank [7].

2.1.2 Heat Transfer

The energy generated in any reaction or bio-reaction must be dissipated to maintain isothermal operation avoiding damages to the microorganisms. The heat transfer is computed using the standard design equation for heat exchangers as follows:

$$Q = U \cdot A \cdot \Delta T \tag{8}$$

where Q is the heat load, A is the contact area, ΔT the temperature gradient and U, the global heat transfer coefficient. U is computed considering the film resistance

inside the vessel, h_i, as well as the film resistance of the jacket, k, and the fluid, h_e [8]. x is the width of the wall and eff are the fouling coefficients.

$$\frac{1}{U} = \frac{1}{h_i} + \text{eff}_{\text{interior}} + \frac{x}{k} + \text{eff}_{\text{exterior}} + \frac{1}{h_e} \tag{9}$$

The internal heat transfer resistance is computed using Eq. (10) for Rushton turbines [8], where k_f is the conductivity, D_a is the diffusion and Pr is the Prandtl number and μ_w is water viscosity as a reference.

$$h_i = \frac{k_f}{D_a} \cdot 0.74 \cdot \text{Re}^{0.67} \cdot \overset{0.33}{\text{Pr}} \left(\frac{\mu}{\mu_w}\right)^{0.14} \tag{10}$$

Likewise, the heat transfer resistance from cooling water flowing inside the jacket can be computed in a similar way as follows:

$$h_e = \frac{k_f}{D_e} \cdot 0.023 \cdot \text{Re}^{0.8} \cdot \overset{0.33}{\text{Pr}} \left(\frac{\mu}{\mu_w}\right)^{0.25} \tag{11}$$

D_e is the diffusion coefficient.

2.2 *Gas-Liquid Systems*

The second main system for the production of alcohols is the fermentation of syngas. This system includes another phase, a gas phase, that must be dispersed in the liquid to provide the feed to the microbial cells. The gas from the bubbles gets dissolved into the liquid phase and is consumed by the cells, which metabolize it to produce ethanol. There are two main bioreactor designs possible for such a fermentation, bubble columns and stirred tank reactors. The former are tanks in which the gas flow injected generates the mixing and the flow pattern inside. The latter are just a modification of the units described for the previous case. A sparger is added to inject the gas phase into the liquid, see Fig. 2. The flow dynamics of gassed stirred tanks depends on both, the stirring and the gas flow.

2.2.1 Hydrodynamics: Gas-Liquid Contact Equipment

- **Bubble Columns**

The hydrodynamics inside a bubble column is generated by the gas injected through the dispersion device. The flow pattern developed depends on the flow rate but also on the bubble size, as well as on the geometry of the equipment and on the

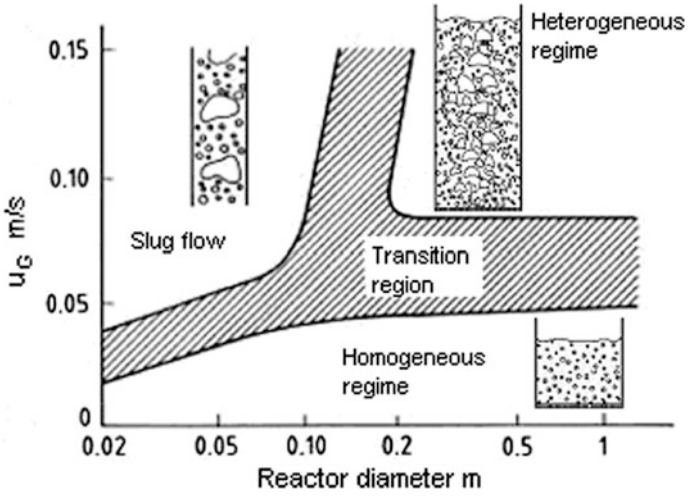

Fig. 3 Flow regimes in a bubble column (Adapted from [9, 10])

physical properties of the liquid. Consequently, three flow regimes are typically found, see Fig. 3. The *homogeneous flow regime* is characterized by a narrow bubble size distribution. The bubbles are distributed across the reactor uniformly. This regime holds up to flow rates of 0.03 m/s, or even as high as 0.08 m/s, depending on the sparger type. As the flow rate increases, the uniform distribution of gas bubbles disappears as turbulent flow develops. This second regime is referred to as the *heterogeneous* or *churn-turbulent flow regime* where a bimodal distribution of bubbles is created. Large bubbles or agglomerates of bubbles form and travel upward at high velocity together with small bubbles which are actually transported downward in a zone close to the column wall. In small diameter bubble columns, like the ones used at laboratory scale, a third regime can be identified, termed slug flow. Slug flow occurs at large flow rates and generates large bubbles that are stabilized at the column wall. Figure 3 shows the three regimes as a function of the superficial gas velocity and the diameter of the column [9, 10].

The bubble dispersion, characterized by equivalent diameter d_{eq}, generated can be characterized by the contact area, a, and the gas hold up, ε_G. The gas hold up refers to the volume of gas within the reactor. Both variables are linked as follows [11]:

$$a = \frac{6\varepsilon_G}{d_{eq}} \tag{12}$$

The area of the gas-liquid interface is one of the most important process parameters at high reaction rates (e.g., when a bubble column is employed as an absorber). Therefore, the interfacial area becomes a crucial factor in equipment

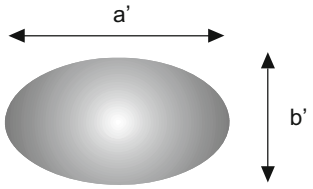

Fig. 4 Equivalent diameter calculations (Eq. 13)

sizing. Like gas hold-up, interfacial area depends on the geometry, the operating conditions, and the gas-liquid system. Mixing deforms the bubbles up to their breaking point, determining the distribution. The equivalent diameter is calculated considering the bubbles as ellipsoids, Fig. 4:

$$d_{eqi} = \left(a'^2 \cdot b'\right)^{(1/3)} \tag{13}$$

The Sauter mean diameter is defined as the ratio between the volume and the surface area and can be computed as follows:

$$d_{32} = \frac{\sum n_i d_{eqi}^3}{\sum n_i d_{eqi}^2} \tag{14}$$

where n_i is the number of bubbles with an equivalent diameter d_{eqi}.

- **Stirred Tank Reactors**

Aside from the use of bubble columns, stirred tanks can also be used for gas-liquid dispersion and mixing. In this case the gas dispersion is generated by combining the gas flow together with the flow pattern generated by the impeller. The two variables that characterize the flow are the dissipated power in the fluid and the gas hold-up. The gas phase affects the mixing and the power consumed. The flow developed by the impeller pushes the bubbles and guides them throughout the tank, against the natural rising tendency of the bubbles (on account of their lower density). This can lead to a great accumulation of gas below the impeller, which will result in hydrodynamic instabilities. In reality, any impeller capable of maintaining the power input in the absence of aeration when the gas phase is introduced will be more stable and its scale-up also be easier. Therefore, each impeller has a particular effect on the gas phase and so the result of the presence of the gas phase on the power input depends on the impeller. For example, it is reported by Vogel and Todaro that Rushton turbines and down flow blades show a reduction in the power input as a result of the gas flow rate [12]. However, concave blades maintain up to 70% of the unaerated power. The equation to compute the aerated power in a gas-liquid system is a modification from the one developed for single phase stirred tanks as follows:

$$P = P_o(RPD)\rho N^3 T^5 \tag{15}$$

where RPD is the relative demand (or the gasification factor) also defined as the ratio between the aerated and the unaerated power input (P_g/P). According to Vogel and Todaro this term depends on the shape of the blades, the gas flow rate, the impeller speed and its diameter [12]. Typical values for the RPD coefficient for Rushton turbines are 0.4, while in the case of concave parabolic blades, it is almost 0.9. If the blades are semi-circular the value is around 0.7. However, when high power is needed, disk turbines with more than 6 blades are used. Turbines with up to 16 blades also result in RPD values around 0.4.

In order to determine the (P_g/P) ratio, empirical correlations based on dimensional analysis have been developed relating the geometrical characteristics of a given impeller to the actual power input. The studied variables have been the stirrer speed, N, the diameter of the stirrer, T, the liquid properties such as density, ρ viscosity, μ, and surface tension, σ, the gas flow, Q. The correlations depend also on dimensionless numbers like the Flow Number of the Weber number [13].The Flow Number, Fl_G, accounts for the effect of the gas phase on the agitation and is defined by Eq. (16) where Q_c is the gas flow rate.

$$Fl_G = \frac{Q_c}{NT^3} \tag{16}$$

For a Rushton turbine, the correlation developed by Hughmark [14], is given by Eq. (17), where V is the volume of the mixture and T_i a blade width:

$$\frac{P_g}{P} = 0.1 \cdot \left(\frac{N^2T^4}{gT_iV^{2/3}}\right)^{-1/5} \cdot \left(\frac{Q_c}{NV}\right)^{-1/4} \tag{17}$$

Alternatively, Michel and Millar proposed another correlation, Eq. (18) [4]:

$$P_g = 0.783\left(\frac{P_o^2NT^3}{Q_c^{0.56}}\right)^{0.459} \tag{18}$$

Finally, design books also present the following Eq. (19):

$$\frac{P_g}{P} = 1 - 1.26 \cdot \frac{Q_c}{NT^3} \tag{19}$$

Although alcohol production will take place in fermentation broth (essentially water), the rheology of the liquid also affects the power input. For instance, pseudoplastic fluids consume less power within a certain range of Reynolds number. Next to the impeller the high velocity gradients result in a small apparent viscosity close to the impeller that increases as the distance from the impeller increases. Thus, the liquid can be in a laminar regime consuming low power.

The power provided by the impeller together with the gas flow rate are responsible for the bubble dispersion and the flow regime, see Fig. 5 [6]. We distinguish three main regimes:

(1) Flooding: The impeller is overwhelmed by the gas and the real contact is poor.
(2) Before loading bubbles rise with little effect from the impeller.
(3) Loading: The impeller can disperse the gas phase through the upper part of the tank.
(4) Complete dispersion: Bubbles are scattered throughout the tank and the gas phase is recycled to the impeller.

In the case of high gas flow rates, the gas phase can remain next to the impeller reducing the power input given by the impeller [15].

Bubble dispersions are characterized by their mean bubble size, $\varepsilon_{G,}$ as well as the specific area. They all play an important role in mass transfer processes since they determine the residence time as well as the contact between the two phases.

The theoretical study of the bubble mean diameter in a gas liquid dispersion has traditionally been analysed according to the Kolmogorov's theory of isotropic turbulence. The maximum stable diameter, $d_{max,}$ for a bubble or a drop is a function of the Weber Number (We) of the system [16].

$$d_{max} = C_1 \cdot We^{-0.6} = C_2 \cdot \varepsilon^{-0.4} = C_3 \cdot N^{-1.2} \tag{20}$$

It is widely accepted that the dispersed energy, ε, corresponds to the power input per unit mass, in all the equations proposed above [17]. Thus, Eq. (20) can be rearranged as follows:

$$d_{max} = C_4 \frac{\sigma^{3/5}}{\rho^{3/5}\varepsilon^{2/5}} \tag{21}$$

where C_i are constants.

The Sauter mean diameter, d_{32}, is considered to be proportional to the maximum stable diameter [16, 18]. Therefore, we can compute d_{32} as follows:

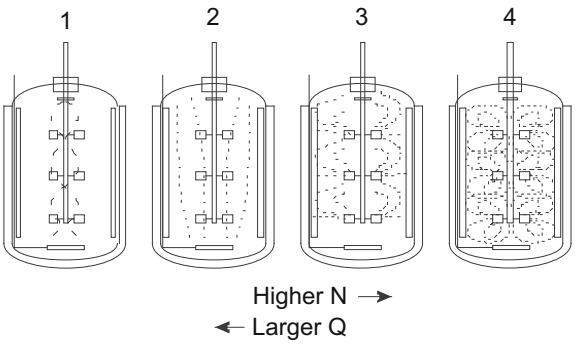

Fig. 5 Flow regimes inside an aerated stirred tank

$$d_{32} = C_5 \frac{\sigma^{3/5}}{\rho^{3/5}\varepsilon^{2/5}} \tag{22}$$

However, Eq. (22) does not include the effect of the gas phase within the tank. Therefore, it was included as in Eq. (23) by Calderbank [18].

$$d_{32} = C_6 \frac{\sigma^{3/5}}{\rho^{3/5}\varepsilon^{2/5}} \varepsilon_G^{1/2} \tag{23}$$

In contrast, if the bubble size is not controlled by the bubble break-up process, the Sauter mean diameter is proportional to the minimum diameter of the bubbles in the dispersion [16]. Therefore,

$$d_{32} = C_7 \cdot \varepsilon^{-0.25} \tag{24}$$

In the equations above, the coefficients C_i are functions of the dispersion device and the impeller type. Thus, to simplify the theoretical considerations, an empirical formula is commonly used, where k_d is an adjustable parameter:

$$d_{32} = k_d \cdot \left(\frac{P_g}{V}\right)^{\delta} \tag{25}$$

This equation has been obtained as the solution to a population balance assuming turbulent break-up of the bubbles whose stability is determined by the surface tension [19]. Several correlations are available in the literature. For example, Bouaifi proposed Eq. (26) for the air-water physical system [20]:

$$d_{32} = 10.1 \times 10^{-3} \cdot \left(\frac{P_g}{V}\right)^{-0.20} \tag{26}$$

The relative volume of gas in the tank is given by the gas hold-up. The empirical equations for the gas hold-up are of the following form [20]:

$$\varepsilon_G = C_1 \left(\frac{P_g}{V}\right)^{\alpha'} u_G^{\beta'} \tag{27}$$

where u_G is the superficial gas velocity. The equation given by Shulka et al. [21] is:

$$\varepsilon_G = C_2 \left[\frac{P_g}{V}(1 - \varepsilon_G)\right]^{\alpha''} u_G^{\beta''} \tag{28}$$

Although more complex correlations have also been developed to include the particular hydrodynamics generated by the impeller (e.g., Kudrewizki and Rabe

[22]), it is also possible to adjust Eq. (28). For Rushton turbines, Gogate et al. [4] presented the following correlation:

$$\varepsilon_G = 0.21\left[\frac{P_g}{V}(1-\varepsilon_G)\right]^{0.27} u_G^{0.65} \tag{29}$$

Using the gas hold-up, we compute the superficial contact area (in a similar way to bubble columns), Eq. (12). Alternatively a theoretical correlation has been proposed based on Kolmogorov's theory, by Calderbank [18]:

$$a = 1.44\left[\frac{(P_g/V)^{0.4}\cdot\rho^{0.2}}{\sigma^{0.6}}\right]\left(\frac{u_G}{U_B}\right)^{0.5} \tag{30}$$

where, U_B is the terminal rising velocity of the bubbles.

2.2.2 Mass Transfer Principles

The gas phase injected into the reactor carries the reactants. The microorganisms are in the liquid phase and the gas must be transported to them. Thus, three stages are to be considered as resistances to the mass transfer, specifically, mass transfer in the gas phase, the mass transfer at the interphase and the mass transfer in the liquid side. The resistances to the mass transfer are also dependent on the hydrodynamics of each phase.

Two film theory: Whitman in 1923 proposed the first attempt to represent the mass transfer between two fluid phases [23]. In his theory, he assumed that there is a laminar layer on each side of the interface between two fluids, while fluid turbulence occurs in the bulk of the phases as can be seen in Fig. 6. In the bulk region, the resistance to mass transfer is negligible due to turbulent eddies and the chaotic movement of the molecules. However, the mass transfer through the laminar film is due to molecular diffusion. As a result, the concentration gradient is linear in the laminar film and zero in the bulk of the phases.

Furthermore, the mass transfer is supposed to be in equilibrium at the interface. As a result, this theory can only be applied in case the concentration gradients are quickly developed compared to the transfer time. Then, using subscript L for the liquid phase, G for the gas phase, B for the fluid bulk and i for the interface, the rate of mass transfer of component A, N_A, is given by:

$$N_A = k_L(c_{LB} - c_{Li}) = k_G(c_{Gi} - c_{GB}) = K(c_{LB} - c_{GB}) \tag{31}$$

where c_{jk} is the concentration of the solute in phase j, k_i and K are the resistances to the mass transfer in the liquid (L), gas (G) phases and the global one. So that:

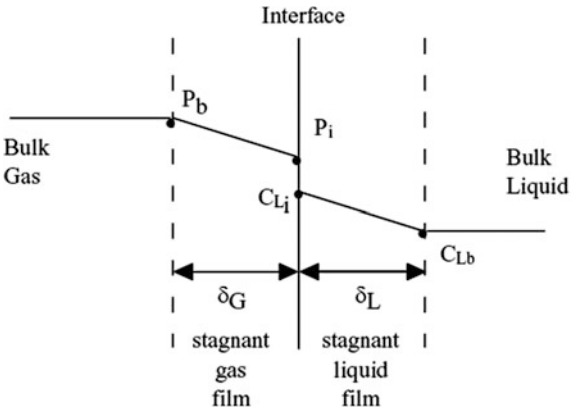

Fig. 6 Two-film theory

$$\frac{1}{K}=\frac{1}{k_L}+\frac{1}{k_G} \tag{32}$$

k_j (j = L, G) depends on the film thickness as well as on the transport properties. The flow determines the film thickness and it is one on the uncertainties of the theory due to the complexity of characterization.

In case the boundary layer is a turbulent, non-slip surface, both molecular and eddy diffusion must be considered, although the latter is bigger and thus presents a negligible resistance [24].

Even though the two film theory considers that there is an equilibrium at the interface and no diffusional resistance, in liquids containing surfactants the diffusional resistance exists, since surfactants locate at the interface. Furthermore, solute diffusion sometimes causes interfacial turbulence unrelated to the flowing liquid mass. This tends to increase the mass transfer rate. Thus, for completion it is considered that the interface is another resistance to the mass transfer and Eq. (33) becomes:

$$N_A = k_L(c_{LB} - c_{Li}) = k_i(c_{Li} - c_{Gi}) = k_G(c_{Gi} - c_{GB}) = K(c_{LB} - c_{GB}) \tag{33}$$

$$\frac{1}{K}=\frac{1}{k_L}+\frac{1}{k_i}+\frac{1}{k_G} \tag{34}$$

Sherwood et al. [24] determined k_i as the maximum mass transfer rate from a gas surface.

$$\frac{1}{k_i}=\frac{\left(2\pi R_g T\right)^{1/2}}{1.006\alpha} \tag{35}$$

α is the fraction of gas molecules colliding with the interface that remains at the liquid phase. $\alpha = 1$ for water, as well as for many simple fluids, and R_g is the gas constant.

It has been experimentally proven that, in gas-liquid processes, the main resistance is usually the resistance of the liquid phase (k_L). Therefore, from now on we present the theory behind predicting k_L. Briefly we discuss three theories:

Penetration theory. Higbie in 1935 developed his theory based on the short contact time between the fluids, resulting in the fact that the concentration gradient does not have the opportunity to reach steady-state [25]. Higbie explained that for a bubble rising through a liquid that absorbs gas, a fluid particle b, initially located on top of the bubble, remains in contact with the gas phase for a time, t, during which the bubble rises a height equal to its diameter. The liquid slips down the bubble. When the contact time is short and the gas diffusion in the liquid phase is slow, solute molecules in solution can never reach a depth equal to z_r, which corresponds to an eddy thickness. Therefore, from the solute point of view the film thickness, z_b is basically infinite [25].

The molar flux of A can be written as:

$$N_A = x_A \cdot (N_A + N_B) - cD_{AB}\nabla x_A \tag{36}$$

where D_{AB} is the diffusion of A into B and x_A is the molar fraction. The unidimensional continuity equation for A is:

$$\frac{\partial c_A}{\partial t} = -\frac{\partial N_{Az}}{\partial z} \tag{37}$$

Combining Eqs. (36) and (37) leads to:

$$N_{Az} = -cD_{AB}\frac{\partial x_A}{\partial z} - x_A\left(\frac{cD_{AB}}{1 - x_{Ao}}\right)\frac{\partial x_A}{\partial z}\bigg|_{z=0} \tag{38}$$

Substituting into Eq. (36)

$$\frac{\partial x_A}{\partial t} = D_{AB}\frac{\partial^2 x_A}{\partial z^2} + \frac{D_{AB}}{1 - x_{Ao}}\frac{\partial x_A}{\partial z}\bigg|_{z=0}\frac{\partial x_A}{\partial z} \tag{39}$$

The equation is solved using:

$$t = 0, x_A = 0; z = 0, x_A = x_{Ao}; z = \infty, x_A = 0 \tag{40}$$

$$k_L = K\sqrt{\frac{D_{AB}}{\pi t}} \tag{41}$$

Physically, this theory states that the liquid eddies are consecutively retained and released from the gas-liquid interface, defining in this way the contact time of the phases [26].

Surface renewal theory: Danckwerts in 1951 pointed out that Higbies's theory (that considers a constant contact time for the turbulent eddies of the liquid at the

gas surface), was a particular case of a more general situation in which eddies are exposed to different time intervals [27]. In reality, the gas-liquid interface is made up of a large number of surface elements with different exposure times. Since solute penetration depends on the exposure time, an average rate must be calculated per unit of surface area by adding the individual values. Danckwerts suggested that surface element replacement was almost independent of the time it had remained at the surface. Hence the fractional replacement rate for the surface elements:

$$N_A = (c_{A,i} - c_{Ao}) \cdot \sqrt{D_{AB} \cdot s} \tag{42}$$

where s is the element replacement rate. From where the mass transfer coefficient k_L is:

$$k_L = \sqrt{D_{AB} \cdot s} \tag{43}$$

So, it was found that k was proportional to $D_{AB}^{0.5}$ [28, 29]. Independently, similar results were obtained by Kishenevsky [30].

Combined theory of surface renewal and film theory: The concept of combined surface renewal and film theory was developed by Dobbins in 1956 [31]. He pointed out that the film theory (which predicted a proportional relationship between k_L and D_{AB}) considered that surface elements are exposed sufficiently such that they generate a steady-state concentration profile in the film. On the other hand, the penetration theory as well as the surface renewal theory, (which predicts a proportionality between k_L and $D_{AB}^{0.5}$) assume that the surface elements are at an infinite depth and, as a result, the diffusing solute will never reach the interior region of constant concentration. The observed dependency collected in the exponent n, depends on the circumstances, and can be explained considering that the surface elements have a finite depth. If z_b is finite:

$$k_L = \sqrt{D_{AB} \cdot s} \coth\left(\sqrt{\frac{s \cdot z_b^2}{D_{AB}}}\right) \tag{44}$$

In this way the exponent n of the diffusivity is within the range of 0.5–1 [28, 29].

Theory for surface stretch: The final theory was developed by Lightfoot and co-workers [32], looking for a trade-off model. They applied the principles of the penetration-surface renewal theory to particular situations where the interfacial surface, through which mass transfer takes place, varies periodically with time. An example of that is an oscillating bubble. A rising bubble oscillates, and if the flow regime inside the bubble column is turbulent, the main mass transfer resistance can be found in the surface layer of changing thickness. A mean volumetric mass transfer coefficient, k_La, with respect to the area is then calculated as:

$$k_L a = \frac{\left(\frac{A_r}{A_{ref}}\right)\sqrt{\frac{D_{AB}}{\pi t}}}{\sqrt{\int_0^{t/t_r}\left(\frac{A_r}{A_{ref}}\right)^2 dt}} \tag{45}$$

where A is the bubble area.

Mass transfer in fluids, **spheres**: In gas-liquid contact equipment, the gas phase is dispersed as bubbles into the liquid phase. In spite of their usually irregular shape, the first approach to study mass transfer from bubbles is to assume that they are spheres. An equation for the mass transfer rate from spheres, whether they are bubbles, drops or solid particles, was proposed by Sherwood et al. in 1975 [24]. For steady-state flow over a submerged spherical particle and considering that only diffusion takes place:

$$\frac{df}{dt} = -D_{AB} \cdot 4\pi r^2 \frac{dc}{dr} \tag{46}$$

where r is the distance from the centre of the particle. Integrating Eq. (46) between limits from the surface, $R = d_b/2$, to infinity:

$$\frac{df}{dt} \cdot \frac{1}{R} = -4 \cdot D_{AB} \cdot \Delta c \tag{47}$$

So that the Sherwood number becomes:

$$Sh = \frac{k d_b}{D_{AB}} \tag{48}$$

where d_b is bubble diameter and k the mass transfer coefficient. And:

$$k \cdot \Delta c = \left(\frac{-1}{A_{ref}}\right)\frac{df}{dt} \tag{49}$$

From Eqs. (47 to 49) it can be calculated that

$$Sh = 2 \tag{50}$$

However, in forced convection the mass transfer rate is reported to be higher than the one predicted by Eq. (50). Therefore, a term related to the contribution of convection is added to the Sherwood number by the Reynolds (Re) and the Schmidt (Sc) numbers to the purely diffusional term as follows:

$$Sh = 2 + C \cdot (Re)^a Sc^{0.33} \tag{51}$$

where the exponent, a, depends on the geometry of the system. However, the exponent of Sc depends on the nature of the diffusional process [33].

Thus, correlations were developed for small and big bubbles as follows as a function of the Grashof, Gr, and Schmidt, Sc, numbers [34]:

$$\text{Big bubbles } (d > 2.5\,\text{mm}) : Sh = 0.42 \cdot (Sc)^{0.5} \cdot (Gr)^{0.33} \tag{52}$$

$$\text{Small bubbles } (d < 0.5\,\text{mm}) : Sh = 2.0 + 0.31 \cdot (Sc \cdot Gr)^{0.33} \tag{53}$$

The liquid film resistance in the interval among big bubbles and small bubbles increases linearly with bubble size according to the experimental results of Calderbank and Moo-Young [34].

Bubble Columns

Experimental results have been fitted to an empirical equation of the form:

$$k_L a = k \cdot u_G^{\beta} \tag{54}$$

Kawase et al. in 1987 proposed that the contact time between phases in Eq. (41) could be considered as the ratio between the length of turbulence, η, and the turbulent velocity, u, defined by the Kolmogorov's theory of isotropic turbulence [35]. Both magnitudes characterize the turbulent flow developed in a stirred tank.

$$\eta = \left(\frac{\nu^3}{\varepsilon}\right)^{1/4} \tag{55}$$

$$u = (\nu \cdot \varepsilon)^{1/4} \tag{56}$$

ν is the kinematic viscosity. The input power per unit mass was determined by $\varepsilon = u_G \cdot g$ [11].

For a Newtonian fluid, combining Eq. (41) and the contact time proposed by Kawase et al. leads to [35]:

$$k_L = \frac{2}{\sqrt{\pi}} \sqrt{D_{AB}} \left(\frac{\varepsilon \rho}{\mu}\right)^{1/4} \tag{57}$$

In the case of a power law fluid, where n and m are the power flow law coefficients:

$$k_L = \frac{2}{\sqrt{\pi}} \sqrt{D_{AB}} \left(\frac{\varepsilon \rho}{m}\right)^{1/(2 \cdot (1+n))} \tag{58}$$

In order to predict, $k_L a$, not only the liquid phase resistance to mass transfer is needed, but also the contact area between the two phases.

Stirred Tank Reactors

The experimental results were fitted to an empirical equation of the form:

$$k_L a = k \cdot \left(\frac{P_g}{V}\right)^{\alpha} \cdot u_G^{\beta} \tag{59}$$

It has been widely used for the study of stirred tanks. In the case of Non-Newtonian fluids, the effective viscosity must also be considered. Modifications to the correlation above can also be found in the scientific literature. However, the various impellers used and the geometric differences between equipment (baffles, configuration of impellers, etc) make it easier to use empirical correlations for each particular system instead of the theories developed to explain and predict $k_L a$, since the effect of the impeller on the bubbles is not considered in any of the available theories.

The first theory to review is that of Barabash and Belevitskaya [36]. The second has already been described above [37], based on Higbies's Theory.

(A) **Barabash's theory for stirred tanks**

Barabash and Belevitskaya in 1995 studied mass transfer from bubbles and drops in turbulent flow in mechanically agitated systems [36]. The theory is based on the relationship between the flow of the liquid and the turbulence in the vicinity of the dispersed phase.

According to the scientific literature, the effect of the turbulence on the mass transfer rate can be studied from two points of view. The first approach is based on the diffusion equation in stationary state in the interface considering the effect of the turbulence at the proximity to the bubble surface. The second uses the non-constant diffusion model near the interface.

Experimentally, it has been verified that the relaxation time (the lifetime of the boundary at the interface) of the surface layer is lower than that necessary for the surface renewal given by the variable diffusion model. Thus, before the surface renewal occurs, the diffusion boundary layer has already reached steady-state and the mass transfer can be approximated by a stationary model at the interface.

Barabash and Belevitskaya showed that, according to experimental data, it is possible to divide the study of $k_L a$ in a stirred tank into three different regions [36]. For power inputs lower than 0.1 W/kg, the mass transfer rate is defined by that of the bubbles rising through a non-stirred fluid. From 0.1 to 1 W/kg, mass transfer increases with the dissipated energy. For higher values of dissipated energy, the $k_L a$ remains constant.

The authors proposed relations for determining $k_L a$ for each region:

Zone 1: **ε<0.1 W/kg**

This region is characterized by low agitation and ε_G lower than 1%.

The mechanism of mass transfer in this region is similar to one in absence of mixing. There is a difference between the mass transfer in the back of the bubble, (β_{rp}), and the front (β_{fp}). For bubbles of 5 mm, the wake of the bubble represents

about 25% of the total surface of the bubble (α_{rp} = 0.25) so that k_La can be calculated by summing the superficial areas .

$$\beta_t = \beta_{rp}\alpha_{rp} + \beta_{fp}(1 - \alpha_{rp}) \tag{60}$$

In order to calculate the value for the frontal region:

$$\beta_{fp} = \frac{0.65 \cdot D_{AB}}{d_b}\sqrt{Re \cdot Sc} \tag{61}$$

For the back part β_s is used.

This region can also be studied from a different approach. Kendoush in 1994 proposed that the bubble shape in these regions was a spherical cap (see Fig. 6) [38]. Using the analogy between heat and mass transfer, in the absence of viscous warming and based on the Higbie theory, he obtained the relationship between the Nusselt, Nu, and the Peclet, Pe, numbers:

$$Nu = Sh = \frac{2}{\sqrt{\pi}}Pe^{0.5} \tag{62}$$

where the eccentricity terms are included as E = 2C/2b (see Fig. 7)

$$Nu = Sh = \frac{2}{\sqrt{\pi}}Pe^{0.5}\left(\frac{3 \cdot E^2 + 4}{E^2 + 4}\right)^{0.5} \tag{63}$$

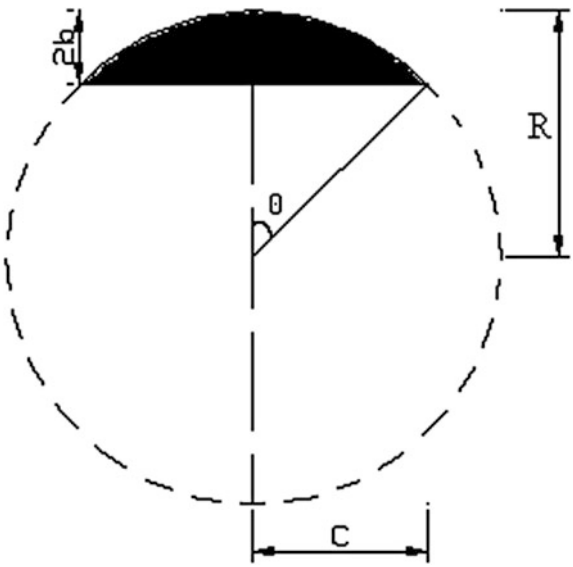

Fig. 7 Dimensions of a bubble cup

The contribution of both regions to the values of Sh and Nu can be calculated as function of the angle θ.

Zone 2: **0.1 <ε< 1 W/kg**

Region 2 is characterized by a change in the average energy dissipation rate. This is a complex zone since there is general turbulence surrounding the bubble as long as pulsations cross the boundary layer. It is assumed that the rear part of the bubble occupies 25% of the bubble surface. Turbulent pulsations whose velocities depend on the energy dissipation rate in the wake zone determine the mass transfer coefficient.

For a certain fraction of the frontal surface (α_{fp}) the averaged velocities of the flow around the bubbles determine the mass transfer rates. For the other part of the frontal surface, the pulsation motion, whose intensity depends on the average value of the energy dissipation rate, determines the value of the mass transfer coefficient.

$$\beta_t = 0.25 \cdot \beta_{rp} + \alpha_{fp} \cdot \beta_{fp} + \left(1 - 0.25 - \alpha_{fp}\right)\beta_0 \tag{64}$$

β_0 is given by Eq. (65) and α_{fp} must be calculated experimentally.

Zone 3: **ε>1 W/kg**

Stationary state in the boundary layer is assumed as well as the relationships for turbulence damping near the surface being distorted.

$$\beta_s = \frac{0.54 \cdot (\varepsilon \cdot \nu)^{0.25}}{Sc^{0.5}} \tag{65}$$

(B) **Kawase's theory**

Kawase and Moo-Young in 1988 derived an expression to determine the k_La based on Higbie's theory [25, 37]. They used Kolmogorov's isotropic turbulence theory to calculate the exposure or contact time.

When the energy dissipated in the tank is high, the surface renewal is more frequent than for the case of a rising bubble. In this case, the liquid film coefficient depends on the turbulent intensity as energy is dissipated. The exposure time can be determined through the dissipated energy.

The contact time can be calculated using Komogorov's theory as the ratio between the two characteristic parameters of the turbulent eddies, their length, η, and the fluctuation velocity, u. Both depend on the dissipated energy per unit mass, ε, and the kinematic viscosity, ν:

$$\eta = \left(\frac{\nu^3}{\varepsilon}\right)^{1/4} \tag{66}$$

$$u = (\nu \cdot \varepsilon)^{1/4} \tag{67}$$

For a Newtonian fluid, the liquid film coefficient is:

$$k_L = \frac{2}{\sqrt{\pi}} \sqrt{D_{AB}} \left(\frac{\varepsilon \rho}{\mu} \right)^{1/4} \tag{68}$$

The energy dissipation is that provided by the impeller. If the liquid obeys the power law:

$$k_L = \frac{2}{\sqrt{\pi}} \sqrt{D_{AB}} \left(\frac{\varepsilon \rho}{m} \right)^{1/(2 \cdot (1+n))} \tag{69}$$

This is the same theory as for bubble columns but, in this case, the dissipated energy is the power input due to the impellers.

2.3 Kinetic Expressions

Monod kinetics is widely used to model the production of bioproducts. The original specific growth rate was

$$\mu = \mu_{max} \frac{S}{K_s + S} \tag{70}$$

where S is the substrate concentration, μ_{max} is the maximum specific growth rate, and K_s, the half velocity constant. Monod also related the yield coefficient to the specific rate of biomass growth, μ, and the rate of substrate utilization (q):

$$\frac{dx}{ds} = Y_{x/s}, \mu = \frac{Y_{x/s}}{X}, q \cong \frac{1}{Y_{x/s}} \frac{ds}{dt} \tag{71}$$

where X is the cells concentration and Y_i are the yield coefficients. This basic model was modified to account for substrate inhibition, K_i, where q_{max} is the maximum rate of substrate utilization:

$$\mu = \mu_{max} \frac{S}{K_s + S + \frac{S^2}{K_i}} \tag{72}$$

$$q = q_{max} \frac{S}{K_s + S + \frac{S^2}{K_i}} \tag{73}$$

A generalized model type of equation is of the form, where S is the substrate concentration and S_m is the critical inhibition concentration. n and m are constants.

$$q = \frac{q_{\max}\left(1 - \frac{S}{S_m}\right)^n}{K_s + S - \left(1 - \frac{S}{S_m}\right)^m} \tag{74}$$

3 Alcohols Production

In this section we present the models for the production of ethanol and biobutanol from sugars and syngas via fermentative processes.

3.1 Ethanol from Sugars

3.1.1 First Generation Ethanol

Ethanol production from corn relies on the fermentation of the sugars produced after breaking down the grain structure. The reaction is exothermic, operating at 32–38 °C under a pressure slightly above atmosphere to secure anaerobic conditions. The fermentation time ranges from 24 to 72 h using *Saccharomyces cerevisiae*. A concentration of ethanol in water no greater than 15% can be achieved. Miller and Melick [39] proposed the following mass balance model for the kinetics where X, S and Et are the cells, substrate and Ethanol concentration, r_i, the kinetic rates, Y_i, the yields and V the mixture volume [39]:

$$\begin{cases} Cells \\ V\frac{dX}{dt} = (r_g - r_d)V \\ Substrate \\ V\frac{dS}{dt} = Y_{s/c}(-r_g)V - r_{sm}V \\ Product \\ V\frac{dEt}{dt} = Y_{p/c}(r_g V) \\ Where \\ r_g = \mu_{max}\left(1 - \frac{Et}{Et^*}\right)^{0.52}\frac{SEt}{K_s + S} \\ r_d = k_d X \\ r_{sm} = mX \\ r_p = Y_{p/c} r_g \end{cases} \tag{75}$$

In Fig. 8 the profiles for the cells, the substrate and the ethanol are presented using the values of:

Et* = 93 g/L; n = 0.52; μ_{max} = 0.33 h^{-1}; K_s = 1.7; $Y_{X/S}$ = 0.08 g/g; $Y_{Et/S}$ = 0.45 g/g; $Y_{Et/X}$ = 0.56 g/g; k_d = 0.01 h^{-1}; m = 0.03 g substrate/(g cells h).

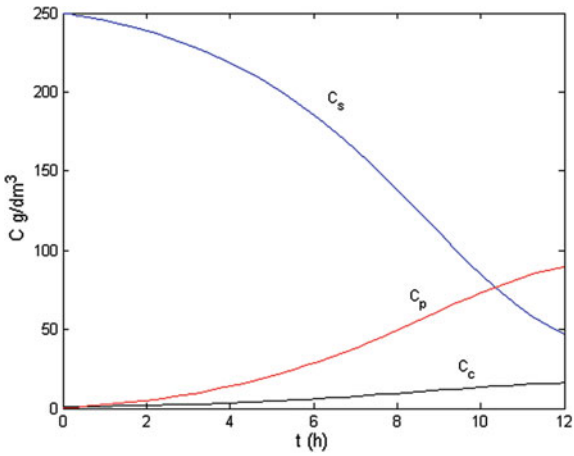

Fig. 8 Species concentration over time

3.1.2 Second Generation Ethanol

It is possible to produce ethanol not only from hexoses but also from pentoses. Second generation ethanol is based on the use of lignocellulosic feedstocks that are composed of a mixture of cellulose, hemicellulose, and lignin. Therefore, the use of both sources of sugars allows a better usage of the crop. However, the fermentation of pentoses is more complex. *Zymomonas mobilis* has been identified as an appropriate microorganism for simultaneously fermenting pentoses and hexoses. Apart from ethanol, other byproducts such as glycerol, succinic acid, acetic acid and lactic acid are also produced. Table 1 shows the reactions and the typical conversions in a second generation bioethanol processes [40].

The reactions to ethanol are exothermic as follows

$$C_6H_{12}O_6 \xrightarrow{\text{yeast}} 2C_2H_5OH + 2CO_2 \quad \Delta H = -84.394\,\text{kJ mol}^{-1}$$

$$3C_5H_{10}O_5 \xrightarrow{\text{yeast}} 5C_2H_5OH + 5CO_2 \quad \Delta H = -74.986\,\text{kJ mol}^{-1}$$

The reaction time is about 24 h at 0.12 MPa to avoid entrance of air. The maximum concentration of ethanol in the water is 6–8%. There are a number of models in the literature for the production of ethanol from xylose and glucose. Here we present one given by Krishnan et al. [41]. the modified Monod kinetics is given as follows:

$$\mu = \frac{\mu_m S}{K_s + S + S^2/K_i} \tag{76}$$

Table 1 Reactions and conversions in a second generation bioethanol production

Reaction	Conversion
Glucose → 2 Ethanol + 2 CO_2	Glucose 0.92
Glucose + 1.2 NH_3 → 6 Z · mobilis + 2.4 H_2O + 0.3 O_2	Glucose 0.04
Glucose + 2 H_2O → Glycerol + O_2	Glucose 0.002
Glucose + 2 CO_2 → 2 Succinic Acid + O_2	Glucose 0.008
Glucose → 3 Acetic Acid	Glucose 0.022
Glucose → 2 Lactic Acid	Glucose 0.013
3 Xylose → 5 Ethanol + 5 CO_2	Xylose 0.8
Xylose + NH_3→ 5 Z · mobilis + 2 H_2O + 0.25 O_2	Xylose 0.03
3 Xylose + 5 H_2O → 5 Glycerol + 2.5 O_2	Xylose 0.02
3 Xylose + 5 CO_2→ 5 Succinic Acid + 2.5 O_2	Xylose 0.03
2 Xylose → 5 Acetic Acid	Xylose 0.01
3 Xylose → 5 Lactic Acid	Xylose 0.01

Next, the product, P, inhibition affecting the growth rate, μ, is included as follows:

$$\frac{\mu}{\mu_0} = \left(1 - \left(\frac{P}{P_m}\right)^{\beta}\right) \tag{77}$$

Thus, the models for the kinetics of the different species involved are as follows, where G represents glucose and X, xylose. The parameters for the fermentation are given in Table 2 [41]. Figure 9 shows the profiles of the main species in the fermentor solving the model given by Eqs. (76)–(79), using the parameters in Table 2.

$$\begin{cases} \text{Cells:} \\ \mu_g = \frac{\mu_{m,g} \cdot S}{K_{s,g} + S + S^2/K_{i,g}} \left(1 - \left(\frac{P}{P_m}\right)^{\beta_g}\right) \\ \mu_x = \frac{\mu_{m,x} \cdot S}{K_{s,x} + S + S^2/K_{i,x}} \left(1 - \left(\frac{P}{P_m}\right)^{\beta_g}\right) \\ \frac{1}{X}\frac{dX}{dt} = \frac{G}{G+X}\mu_g + \frac{X}{G+X}\mu_x \end{cases} \tag{78}$$

$$\begin{cases} \text{Product:} \\ v_{E,g} = \frac{v_{m,g} \cdot S}{K_{s,g} + S + S^2/K_{i,g}} \left(1 - \left(\frac{P}{P_m}\right)^{\gamma_g}\right) \\ v_{E,x} = \frac{v_{m,x} \cdot S}{K_{s,x} + S + S^2/K_{i,x}} \left(1 - \left(\frac{P}{P_m}\right)^{\gamma_x}\right) \\ \frac{1}{X}\frac{dP}{dt} = (v_{E,x} + v_{E,g}) \end{cases} \text{ with } \begin{cases} \mu_{m,g} = 0.152 \cdot X^{-0.461} \\ \mu_{m,x} = 0.075 \cdot X^{-0.438} \\ v_{m,g} = 1.887 \cdot X^{-0.434} \\ v_{m,x} = 0.16 \cdot X^{-0.233} \end{cases}$$

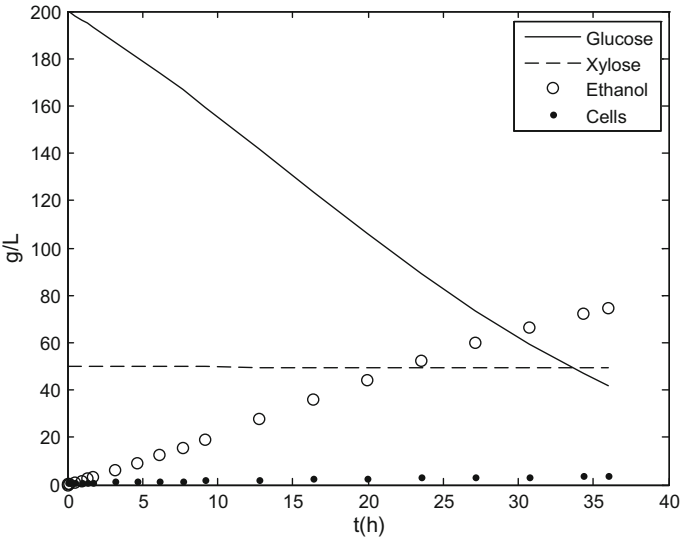

Fig. 9 Ethanol production from hexoses and pentoses [42]

Table 2 Kinetic parameters for fermentation

Parameter	Glucose fermentation	Xylose fermentation
μ_m (h^{-1})	0.662	0.190
ν_m (h^{-1})	2.005	0.250
K_S (g/L)	0.565	3.400
K_S' (g/L)	1.342	3.400
K_i (g/L)	283.700	18.100
K_i' (g/L)	4890.000	81.300
P_m (g/L)	95.4 for $P \leq 95.4$ g/L	
	129.9 for $95.4 \leq P \leq 129$ g/L	59.040
P_m' (g/L)	103 for $P \leq 103$ g/L	
	136.4 for $103 \leq P \leq 136.4$ g/L	60.200
β	1.29 for $P \leq 95.4$ g/L	
	0.25 for $95.4 \leq P \leq 129$ g/L	1.036
γ	1.42 for $P \leq 95.4$ g/L	0.608
m (h^{-1})	0.097	0.067
$Y_{P/S}$ (g/g)	0.470	0.400
$Y_{X/S}$ (g/g)	0.115	0.162

$$\begin{cases} \text{Sustrate:} \\ -\frac{dS}{dt} = \frac{1}{Y_{X/S}}\frac{dX}{dt} + mX = \frac{1}{Y_{P/S}}\frac{dP}{dt} \\ -\frac{dS}{dt} = \frac{1}{Y_{P/S}}\frac{dP}{dt} \\ -\frac{dxylo}{dt} = \frac{1}{Y_{P/S}}(v_{E,x}X) \\ -\frac{dglu}{dt} = \frac{1}{Y_{P/S}}(v_{E,g}X) \end{cases} \tag{79}$$

3.2 Ethanol from Syngas

Second generation ethanol can also be based on gaseous feedstocks. Syngas, a mixture of CO and H_2, can be used in the well-known Fischer-Tropsch reaction, followed by a catalytic synthesis to produce a mixture of alcohols. Alternatively, syngas can also be fermented. The groups of microorganisms that can synthesize valuable products from syngas are known as acetogens. They ferment the gas through the reductive acetyl-CoA pathway with acetate as their main product. Among them we can find the most well studied examples such as *Acetobacterium woodii*, *Alkalibaculumbacchi*, *Butyribacterium methylotrophicum*, *Clostridium aceticum*, *Clostridium ljungdahlii*, *Clostridium thermoaceticum*, *Clostridium autoethanogenum*, *Clostridium ragsdalei* and *Clostridium carboxidivorans* [43–45].

This fermentation also takes place at 32–38 °C and pH 4–6, also under anaerobic conditions. It is an exothermic reaction that follows the stoichiometry below. The conversion of the H_2 (or CO since H_2:CO = 1) is about 70%. The unconverted gas can be used as a fuel or cleaned and recycled [46].

$$3CO + 3H_2 \rightarrow C_2H_5OH + CO_2$$

For the reaction to operate, inhibitor species from the raw syngas must be removed such as H_2S, NH_3(and even O_2), which are common in small amounts in the output from gasification plants. The use of pressure swing absorption, with alkali absorbents (such as monoethanolamine, MEA) are typically used to clean up the gas [46]. Once in the reactor, the first key limitation in the fermentation of syngas is the maximum concentration of ethanol. The best current practice claims a maximum concentration of ethanol in the reactor of 5% [47]. Due to this well-established problem, new systems are in development to adsorb ethanol from the water during the synthesis reducing the concentration so that the bacteria can produce more ethanol [48], using in-situ product removal technologies [49].

Until recently, another issue when generating ethanol from syngas has been the production of the by-product acetic acid. In the nineties, it was already possible to obtain high selectivity towards ethanol [50, 51]. BRI and Coskata industries have recently reported that their bacteria are capable of producing only ethanol [52]. In the scientific literature there are several models presenting the kinetics of ethanol production from syngas. For example, Chen et al. present a

Table 3 Stoichiometry of growth and product formation by *C. ljungdahlii* ($\nu_{i,j}$)

	CO (mol L^{-1})	CO_2 (mol L^{-1})	H_2 (mol L^{-1})	Biomass (X) (mol L^{-1})	Acetate (mol L^{-1})	Et (mol L^{-1})	
Biomass growth on CO	$-1/Y_1$	$0.5/Y_1 - 0.0175$		1	$0.25/Y_1 - 0.5$		(1)
Biomass growth on CO_2 and H_2		$-(0.5/Y_2 - 0.0175)$	$-1/Y_2$	1	$0.25/Y_2 - 0.5$		(2)
Ethanol production from CO	$-1/Y_3$	$0.67/Y_4$				1	(3)
Ethanol production from CO_2 and H_2		$-0.33/Y_4$	$-1/Y_4$			1	(4)
Conversion of acetate into ethanol CO	$-2/Y_5$	$2/Y_5$			$-1/Y_5$	1	(5)
Conversion of acetate into ethanol H_2			$-2/Y_6$		$-1/Y_6$	1	(6)

simple model based on the rate of CO consumption [53]. In this section we present the model by Vandecasteele [54] for completeness divided into bioconversion reactions and the balance to the gas phase. Table 3 shows the stoichiometry of the fermentation:

The kinetics of the reactions above are given as follows:

$$\begin{cases} \rho_1 = \mu_1^{\max} \dfrac{C_{CO}}{K_{CO} + C_{CO} + \frac{C_{CO}^2}{K_{I,CO}}} \cdot \dfrac{K_{I,UA}}{K_{I,UA} + C_{UA}} X \\ \rho_2 = \mu_2^{\max} \dfrac{C_{CO_2}}{K_{CO_2} + C_{CO_2}} \cdot \dfrac{C_{H_2}}{K_{H_2} + C_{H_2}} \cdot \dfrac{K_{I,CO}^{hy}}{K_{I,CO}^{hy} + C_{CO}} \cdot \dfrac{K_{I,UA}}{K_{I,UA} + C_{UA}} X \\ \rho_3 = \mu_3^{\max} \dfrac{C_{CO}}{K_{CO} + C_{CO} + \frac{C_{CO}^2}{K_{I,CO}}} \cdot \dfrac{C_{UA}}{K_{UA} + C_{UA}} X \\ \rho_4 = \mu_4^{\max} \dfrac{C_{CO_2}}{K_{CO_2} + C_{CO_2}} \cdot \dfrac{C_{H_2}}{K_{H_2} + C_{H_2}} \cdot \dfrac{K_{I,CO}^{hy}}{K_{I,CO}^{hy} + C_{CO}} \cdot \dfrac{C_{UA}}{K_{UA} + C_{UA}} X \\ \rho_5 = \mu_5^{\max} \dfrac{C_{CO}}{K_{CO} + C_{CO} + \frac{C_{CO}^2}{K_{I,CO}}} \cdot \dfrac{C_{UA}}{K_{UA}^{ac} + C_{UA}} X \\ \rho_6 = \mu_6^{\max} \dfrac{C_{H_2}}{K_{H_2} + C_{H_2}} \cdot \dfrac{C_{UA}}{K_{UA}^{ac} + C_{UA}} \cdot \dfrac{K_{I,CO}^{hy}}{K_{I,CO}^{hy} + C_{CO}} X \end{cases} \tag{80}$$

See Table 4 for the definition of the terms and the constants involved in the rates above.

Gas phase mass balances (i is the component as in Table 4). It is assumed that the gas is fed to the volume above the liquid, V_G, for simplicity in the model development. That volume is assumed to be constant so, we can compute the partial pressure of the gases assuming ideal behavior and no reaction in the gas phase, no evaporation of water or ethanol:

Table 4 Values for the constants in the mass balances and kinetic rates

Symbol	Description	Value	Unit
Yield coefficients			
Y_1	Cell yield of carbon monoxide	0.0257	Mol cell (mol CO)$^{-1}$
Y_2	Cell yield to hydrogen	0.0068	Mol cell (mol H_2)$^{-1}$
Y_3	Ethanol yield to carbon monoxide	0.167	Mol ethanol (mol CO)$^{-1}$
Y_4	Ethanol yield of hydrogen	0.167	Mol ethanol (mol H_2)$^{-1}$
Y_5	Ethanol yield of acetate (CO)	1	Mol ethanol (mol acetate)$^{-1}$
Y_6	Ethanol yield of acetate ($H_{2)}$	1	Mol ethanol (mol acetate)$^{-1}$
Parameters			
μ_1^{max}	Maximum specific growth rate from CO	0.195	Mol cell (mol cell)$^{-1}$ h^{-1}
		0.022	
		0.04	
μ_2^{max}	Maximum specific growth rate from CO_2 and H_2	0.042	Mol cell (mol cell)$^{-1}$ h^{-1}
μ_3^{max}	Maximum specific ethanol production from CO	0.39	Mol ethanol (mol cell)$^{-1}$ h^{-1}
μ_4^{max}	Maximum specific ethanol production from CO_2 and H_2	0.39	Mol ethanol (mol cell)$^{-1}$ h^{-1}
μ_5^{max}	Maximum specific acetate conversion rate from CO	0.39	Mol ethanol (mol cell)$^{-1}$ h^{-1}
μ_6^{max}	Maximum specific ethanol production from CO_2 and H_2	0.39	Mol ethanol (mol cell)$^{-1}$ h^{-1}
K_{CO}	CO saturation constant	0.000078	M
		0.00069	
K_{CO_2}	CO_2 saturation constant	0.00022	M
K_{H2}	H_2 saturation constant	0.00022	M
		0.0003	
K_{UA}	UA saturation constant for ethanol production	0.0005	M
K_{UA}^{ac}	UA saturation constant for acetate conversion	0.0005	M
$K_{I,CO}$	CO inhibition constant	0.002	M
		0.00048	
$K_{I,CO}^{ky}$	CO inhibition constant for hydrogenate	0.000000007	M
$K_{I,UA}$	UA inhibition constant	0.00062	M
X_{Max}	Maximum biomass concentration before total sporulation	0.0009631	M
α	Inhibition coefficient	1	

$$\begin{cases} \frac{d(V_G \cdot C_{G,i})}{dt} = -k_L a_i (C^*_{L,i} - C_{L,i}) V_L \\ n_G = V_G \sum_i C_{G,i} \\ p = \frac{n_G RT}{V_G} \\ p_i = \frac{V_G C_{G,i}}{n_G} p \end{cases} \tag{81}$$

Liquid phase mass balances

$$\begin{cases} \frac{d(V_L \cdot C_{L,i})}{dt} = -k_L a_i (C^*_{L,i} - C_{L,i}) V_L + r_i V_L \\ r_i = \sum_{i=1}^{6} \upsilon_{i,j} \rho_j \\ \frac{d(C_{L,i})}{dt} = -k_L a_i (C^*_{L,i} - C_{L,i}) + r_i \\ V_L = cte \end{cases} \tag{82}$$

Taking into account that there is no physical transport of biomass and products

$$\begin{cases} \frac{dC_X}{dt} = r_X = (\mu_{X1} + \mu_{X2}) X \\ \frac{dC_A}{dt} = r_A = \left[\left(\frac{0.25}{Y_{X1}} - 0.5 \right) (\mu_{X1} + \mu_{X2}) - \frac{\mu_{e3}}{Y_{e3}} - \frac{\mu_{e4}}{Y_{e4}} \right] X \\ \frac{dC_E}{dt} = r_E = [(\mu_{e1} + \mu_{e2} + \mu_{e3} + \mu_{e4})] X \end{cases} \tag{83}$$

The conversion rates of carbon monoxide, carbon dioxide and hydrogen can be calculated by the summation of the products of the reaction rates and their respective stoichiometric coefficients:

$$\begin{cases} \frac{dC_{CO}}{dt} = r_{CO} = \left[-\frac{\mu_{X1}}{Y_{X1}} - \frac{\mu_{e1}}{Y_{e1}} - \frac{2\mu_{e3}}{Y_{e3}} \right] X \\ \frac{dC_{CO_2}}{dt} = r_{CO_2} = \left[\left(\frac{0.5}{Y_{X1}} - 0.0175 \right) (\mu_{X1}) - \left(\frac{0.5}{Y_{X2}} - 0.0175 \right) (\mu_{X2}) + \frac{0.67\mu_{e1}}{Y_{e1}} - \frac{0.33\mu_{e2}}{Y_{e2}} + \frac{2\mu_{e3}}{Y_{e3}} \right] X \\ \frac{dC_{H_2}}{dt} = r_{H_2} = \left[-\frac{\mu_{X2}}{Y_{X2}} - \frac{\mu_{e2}}{Y_{e2}} - \frac{2\mu_{e4}}{Y_{e4}} \right] X \end{cases} \tag{84}$$

The liquid mass balances of the gaseous substrates and nitrogen gas are as follows.

$$\begin{cases} \frac{dC_{L,CO}}{dt} = k_L a_{CO} \cdot (C^*_{L,CO} - C_{L,CO}) + r_{CO} \\ \frac{dC_{L,CO_2}}{dt} = k_L a_{CO_2} \cdot (C^*_{L,CO_2} - C_{L,CO_2}) + r_{CO_2} \\ \frac{dC_{L,H_2}}{dt} = k_L a_{H_2} \cdot (C^*_{L,H_2} - C_{L,H_2}) + r_{H_2} \\ \frac{dC_{L,N_2}}{dt} = k_L a_{N_2} \cdot (C^*_{L,N_2} - C_{L,N_2}) \end{cases} \tag{85}$$

To compute the saturation concentrations, C^*, we assume Henry's Law, see Table 5.

Table 5 Henry's coefficients (k_H)

Components	Value (mol L^{-1} atm^{-1})
CO	8.30×10^{-4}
CO_2	2.45×10^{-2}
H_2	7.32×10^{-4}
N_2	5.48×10^{-4}

$$C^*_{L,i} = p_i \cdot k_{H,i} \tag{86}$$

While the mass transfer coefficient was corrected from the one experimentally determined for CO_2 using Higbies's theory

$$k_L a_i = k_L a_{CO_2} \sqrt{\frac{D_i}{D_{CO_2}}} \tag{87}$$

3.3 Biobutanol

Most of the work in the scientific literature about biofuel production is focused on the production of bioethanol as the alcohol of choice. However, biobutanol is an interesting alternative, not least because it has better properties. For years it has been produced following the so-called ABE (acetone-butanol-ethanol) fermentation. The production of the three products simultaneously results in a low yield of butanol, reducing the economic attractiveness of the system. Only recently Malmierca et al. [55] have developed a process based on an AB fermentation where by integrating fermentation with pervaporation, a high yield of butanol is produced [55]. Additionally, the product stream contains solely acetone and butanol. In this section we present the mechanism and kinetics of typical ABE fermentations from glucose and xylose. There are several models in the literature but among the most complete is the one by Shinto et al. [56], Raganati et al. [57]. We refer to the original paper for further explanation of the model due to the large number of intermediates involved in the kinetics such as fructose-6-phosphate (F6P), glyceraldehyde-3-phosphate (G3P), acetyl-CoA (AcoA), butyryl-CoA (BCoA),acetoacetyl-CoA (AACoA), xylulose-5-phosphate (X5P), sedoheptulose-7-phosphate (S7P), erythrose-4-phosphate (E4P),ribose-5-phosphate(R5P). K_i are half live velocities and V_i are the specific growth rates. F is a binary term that inactivates that part of the model and is equal to 1 if the xylose concentration is over 1 mM and 0 otherwise:

$$
\begin{cases}
r_1 = \frac{V_{\max 1}[Glucose][Biomass]}{K_{m1} + K_{m1}([Glucose]/K_{is1})^2 + [Glucose](1 + [Butanol]/K_{ii1})} F \\
r_2 = \frac{V_{\max 2}[F6P][Biomass]}{K_{m2} + [F6P]} F \\
r_3 = \frac{V_{\max 3}[G3P][Biomass]}{K_{m3} + [G3P]} F \\
r_4 = \frac{V_{\max 4}[Lactate][Biomass]}{K_{m4} + [Lactate]} F \\
r_5 = \frac{V_{\max 5}[Pyruvate][Biomass]}{K_{m5} + [Pyruvate]} F \\
r_6 = \frac{V_{\max 6}[Pyruvate][Biomass]}{K_{m6} + [Pyruvate]} F \\
r_7 = \frac{V_{\max 7}[Acetate][Biomass]}{K_{m7} + [Acetate]} F \\
r_8 = V_{\max 8} \left(\frac{1}{1 + (K_{m8A}/[Acetate])} \right) \left(\frac{1}{1 + (K_{m8B}/[AACoA])} \right) [Biomass] \\
r_9 = \frac{V_{\max 9}[ACoA][Biomass]}{K_{m9} + [ACoA]} F \\
r_{10} = \frac{V_{\max 10}[ACoA][Biomass]}{K_{m10} + [ACoA]} F \\
r_{11} = \frac{V_{\max 11}[ACoA][Biomass]}{K_{m11} + [ACoA]} F \\
r_{12} = \frac{V_{\max 12}[ACoA][Biomass]}{K_{m12}(1 + [Butanol]/K_{ii12}) + [ACoA](1 + [Butanol]/K_{ii12})} \\
r_{13} = k_{13}[Biomass] \\
r_{14} = \frac{V_{\max 14}[AACoA][Biomass]}{K_{m14} + [AACoA]} F \\
r_{15} = V_{\max 15} \left(\frac{1}{1 + (K_{m15A}/[Butyrate])} \right) \left(\frac{1}{1 + (K_{m15B}/[AACoA])} \right) [Biomass] \\
r_{16} = \frac{V_{\max 16}[Acetoacetate][Biomass]}{K_{m16} + [Acetoacetate]} \\
r_{17} = \frac{V_{\max 17}[Butyrate][Biomass]}{K_{m17} + [Butyrate]} F \\
r_{18} = \frac{V_{\max 18}[BCoA][Biomass]}{K_{m18} + [BCoA]} F \\
r_{19} = \frac{V_{\max 19}[BCoA][Biomass]}{K_{m19} + [BCoA]} F \\
r_{20_X} = \frac{V_{\max 20}[Xylose][Biomass]}{K_{m20}(1 + [Xylose]/K_{is20}) + [Xylose](1 + [Butanol]/K_{ii20})} F \\
r_{21_X} = \frac{V_{\max 21}[X5P][Biomass]}{K_{m14} + [X5P]} \\
r_{22_X} = \frac{V_{\max 22}[R5P][Biomass]}{K_{m22} + [R5P]} \\
r_{23_X} = V_{\max 23} \left(\frac{1}{1 + (K_{m23A}/[R5P])} \right) \left(\frac{1}{1 + (K_{m23B}/[X5P])} \right) [Biomass] \\
r_{24_X} = V_{\max 24} \left(\frac{1}{1 + (K_{m24A}/[S7P])} \right) \left(\frac{1}{1 + (K_{m24B}/[G3P])} \right) [Biomass] \\
r_{25_X} = V_{\max 25} \left(\frac{1}{1 + (K_{m25A}/[X5P])} \right) \left(\frac{1}{1 + (K_{m25B}/[E4P])} \right) [Biomass]
\end{cases}
\tag{88}
$$

$$
\begin{cases}
\frac{d[Glucose]}{dt} = -r_1 \\
\frac{d[F6P]}{dt} = r_1 - r_2 \\
\frac{d[G3P]}{dt} = r_2 - r_3 \\
\frac{d[Pyruvate]}{dt} = r_3 + r_4 - r_5 - r_6 \\
\frac{d[Lactate]}{dt} = r_5 - r_4 \\
\frac{d[ACoA]}{dt} = r_6 + r_7 + r_8 - r_9 - r_{10} - r_{11} - r_{12} \\
\frac{d[Biomass]}{dt} = r_{12} - r_{13} \\
\frac{d[Acetate]}{dt} = r_9 - r_7 - r_8 \\
\frac{d[Ethanol]}{dt} = r_{11} \\
\frac{d[AACoA]}{dt} = r_{10} - r_8 - r_{14} - r_{15} \\
\frac{d[Acetoacetate]}{dt} = r_8 + r_{15} - r_{16} \\
\frac{d[BCoA]}{dt} = r_{14} + r_{15} + r_{17} - r_{18} - r_{19} \\
\frac{d[Butyrate]}{dt} = r_{18} - r_{15} - r_{17} \\
\frac{d[Acetone]}{dt} = r_{16} \\
\frac{d[CO_2]}{dt} = r_6 + r_{16} \\
\frac{d[Butanol]}{dt} = r_{19} \\
\frac{d[Xylose]}{dt} = -r_{20_X} \\
\frac{d[X5P]}{dt} = r_{20_X} + r_{22_X} - r_{21_X} \\
\frac{d[R5P]}{dt} = r_{21_X} - r_{22_X} - r_{23_X} \\
\frac{d[S7P]}{dt} = r_{23_X} - r_{24_X} \\
\frac{d[E4P]}{dt} = r_{24_X} - r_{25_X} \\
\frac{d[F6P]}{dt} = r_{24_X} + r_{25_X} + r_{2_X} \\
\frac{d[G3P]}{dt} = r_{2_X} + r_{25_X} - r_{3_X} - r_{24_X}
\end{cases}
\tag{89}
$$

Table 6 shows the coefficients for the previous equations.

4 Conclusions

In this chapter we have provided an overview of the principles and the design of fermenters devoted to the production of alcohols such as ethanol and butanol. We cover the production of first generation ethanol from glucose, second generation ethanol either from sugars, glucose and xylose, or syngas and finally butanol via ABE fermentation from sugars. The chapter presents the hydrodynamics of the tanks, single phase and multiphase gas-liquid type tanks, the heat and mass transfer characteristics as well as the kinetic expressions. Finally, a sample kinetics of each of the above mentioned cases is presented. Single phase bioreactors are typically used for sugar based alcohols production. The presence of the alcohols in the mixture inhibits the reaction and therefore the kinetics is complex following Monod models.

Table 6 Coefficients for butanol production kinetics

Reaction	K (h^{-1})	V_{Max} (h^{-1})	K_m (mM)	K_{is} (mM)	K_{ii} (mM)	K_a (mM)	K_{mA} (mM)	K_{mB} (mM)
R1		3.2	46.0	55.6	67.5			
R2		40.0	10.0					
R3		120	26.5					
R4		7.50	177					
R5		9.70	500					
R6		180	1.50					
R7		0.30	50.0					
R8		19.0					40.0	70.0
R9		26.5	51.0					
R10		20.0	1.00					
R11		7.45	30.0					
R12		8.10	1.10		23.0			
R13	0.017							
R14		10.0	5.20					
R15		80.0					15.0	50.0
R16		12.0	10.0					
R17		35.0	4.90			2.20		
R18		100	6.10					
R19		3.15	5.00		67.5	2.20		
R20		1.09	0.026	0.126	0.014			
R21		0.83	0.026	0.126	0.014			
R22		45.0					0.05	0.0025
R23		45.0					0.05	0.0025
R24		45.0					0.05	0.0025
R25		65.0					0.05	0.0025

Alternatively, syngas can be fermented to ethanol. These reactors are two phase ones where the mass transfer from the gas to the liquid is the limiting stage. Hydrodynamics are responsible for the contact between the reactants and the liquid and several reactor designs are available, from bubble columns to CSTR's.

References

1. Walas SM (1990) Chemical process equipment. Selection and design. Butterworth-Heinemann, Boston
2. Martín M, Montes FJ, Galán MA (2008) Bubbling process in stirred tank reactors I: agitator effect on bubble size, formation and rising. Chem Eng Sci 63:3212–3222
3. Nienow AW (1997) On impeller circulation and mixing effectiveness in the turbulent flow regime. Chem Eng Sci 52(15):2557–2565

4. Gogate PR, Beenackers AACM, Pandit AB (2000) Multiple-impeller systems with a special emphasis on bioreactors: a critical review. Biochem Eng J 6:109–144
5. Joshi JB, Pandit AB, Sharma MM (1982) Mechanically agitated gas-liquid reactors. Chem Eng Sci 37(6):813–844
6. Harnby N, Edwards MF, Nienow AW (1992) Mixing in the process industries, 2nd edn. Butterworth-Heinemann, Oxford
7. McCabe WL, Smith JC, Harriot P (1985) Unit operations of chemical engineering. McGraw-Hill Book Company, Singapore
8. Sinnott RK (1999) In: Coulson, Richardson (eds) Chemical engineering, 3rd edn. Butterworth Heinemann, Singapore
9. Zehner P, Kraume M (2000) Bubble columns. Ullmann's encyclopedia of industrial chemistry (Online)
10. Krishna R (2000) A scale up strategy for a commercial scale bubble column slurry reactor Fischer-Tropsch synthesis. Oil Gas Sci Tech 55(4):359–393
11. Shimizu K, Takada S, Minekawa K, Kawase Y (2000) Phenomenological model for bubble column reactors prediction of gas hold-ups and volumetric mass transfer coefficients. Chem Eng Sci 78:21–28
12. Vogel HC, Todaro CL (1996) Fermentation and biochemical engineering handbook: principles, process design and equipment, Chapter 5. Noyes Publications, New Jersey
13. Hassan ITM, Robinson CW (1977) Stirred-tank mechanical power requirement and has holdup in aerated aqueous phases. AIChE J 23:48–56
14. Hughmark GA (1980) Power requirements and interfacial area in gas liquid turbine agitated systems. Ind Eng Chem Proc Des Dev 19:638–641
15. Paul EL, Atiemo OVA, Kresta SM (2004) Handbook of industrial mixing. Wiley-Interscience, New York
16. Pacek AW, Man CC, Nienow AW (1998) On the sauter mean diameter and size distributions in turbulent liquid/liquid dispersions in a stirred vessel. Chem Eng Sci 53:2005–2011
17. Alves SS, Maia CI, Vasconcelos JMT (2002) Experimental and modeling study of gas dispersion in a double turbine stirred tank. Chem Eng Sci 57:487–496
18. Calderbank PH (1958) The interfacial area in gas liquid contacting with mechanical agitation. Trans Inst Chem Eng 36:443–463
19. Galindo E, Pacek AW, Nienow AW (2000) Study of drop and bubble sizes in a simulated mycelial fermentation broth of up to four phases. Biotechnol Bioeng 69(2):213–227
20. Bouaifi M, Hebrard G, Bastoul D, Roustan M (2001) A comparative study of gas hold up, bubble size, interfacial area and mass transfer coefficients in stirred gas liquid reactors and bubble columns. Chem Eng Process 40:97–111
21. Shukla VB, Veera UP, Kulkarni PR, Pandit AB (2001) Scale up of biotransformation process in stirred tank reactor using dual impeller bioreactor. Biochem Eng J 8:19–29
22. Kudrewizki F, Rabe P (1986) Model of the dissipation of mechanical energy in gassed stirred tanks. Chem Eng Sci 41:2247–2252
23. Whitman WG (1923) The two-film theory of absorption. Chem Met Eng 29:146–148
24. Sherwood TK, Pingford RL, Wilke CR (1975) Mass transfer. Chemical Engineering Series. McGraw Hill, New York
25. Higbie R (1935) The rate of absorption of a pure gas into a still liquid during a short time of exposure. Trans Am Ins Chem Eng 31:365–389
26. Miller DN (1974) Scale-up of agitated vessels gas-liquid mass transfer. AIChE J 20(3):445–453
27. Danckwerts PV (1951) Significance of liquid-film coefficients in gas absorption. Ind Eng Chem 43:1460–1467
28. Treybal RE (1990) Operaciones de transferencia de masa, Chapter 3, 2nd edn. McGraw Hill, México
29. Skelland AHP (1974) Diffusional mass transfer. Wiley, New York

30. Kafarov V (1975) Fundamentals of mass transfer: gas liquid, Vapour-Liquid and liquid-liquid systems. Mir Publishers, Moscow
31. Dobbins WE (1956) The nature of the oxygen transfer coefficient in aeration systems. Biological treatment of sewage and industrial wastes, 1, 2-1. Reinhold, New York, pp 141–148
32. Angelo JB, Lightfoot EN, Howard DW (1966) Generalization of the penetration theory for surface stretch: application to forming and oscillating drops. AIChE J 12:751–760
33. Davies JT (1972) Turbulence phenomena. Academia Press, New York, pp 143–144
34. Calderbank PH, Moo-Young MB (1961) The continuous phase heat and mass transfer properties of dispersions. Chem Eng Sci 16:39–54
35. Kawase Y, Halard B, Moo-Young M (1987) Theoretical prediction of volumetric mass transfer coefficients in bubble columns for Newtonian and non-Newtonian fluids. Chem Eng Sci 42:1609–1617
36. Barabash VM, Belevitskaya MA (1995) Mass transfer from bubbles and drops in mechanically agitated apparatuses. Theor Found Chem Eng 29(4):333–342
37. Kawase Y, Moo-Young M (1988) Volumetric mass transfer coefficients in aerated stirred tank reactors with Newtonian and non-Newtonian media. Chem Eng Res Des 66:284–288
38. Kendoush AA (1994) Theory of convective heat and mass transfer to spherical cap bubbles. AIChE J 40(9):1440–1448
39. Miller R, Melick M (1987) Chem Eng 113
40. Aden A, Foust T (2009) Techno economic analysis of the dilute sulfuric acid and enzymatic hydrolysis process for the conversion of corn stover to ethanol. Cellulose 16(4):535–545
41. Krishnan MS, Ho NWY, Tsa GT (1999) Fermentation kinetics of ethanol production from glucose and xylose by recombinant *Saccharomyces* 1400 (pLNH33). Appl Biochem Biotech 77–79:373–388
42. Martín M (2016) Industrial chemical process analysis and design. Elsevier, Oxford
43. Munasinghe PC, Khanal SK (2011) Biomass-derived syngas fermentation into biofuels. Biofuels 101(13):79–98
44. Mohammadi M, Najafpour GD, Younesi H, Lahijani P, Uzir MH, Mohamed AR (2011) Bioconversion of synthesis gas to second generation biofuels: a review. Renew Sustain Energy Rev 15(9):4255–4273
45. Madigan MT, Martinko JM, Stahl DA (2012) Biology of microorganisms, 13th edn. Benjamin Cummings
46. Martín M, Grossmann IE (2011) Energy optimization of bioethanol production via gasification of switchgrass. AIChE J 57(12):3408–3428
47. Van Kasteren JMN, Dizdarevic D, Van der Waall WR, Guo J, Verberne R (2005) Bio-ethanol from bio-syngas. Technical Report. Technische Universiteit Eindhoven (TU/e), Telos &Ingenia Consultants & Engineers No 0456372-R02
48. Nielsen DR, Prather KJ (2009) Adsorption of second generation biofuels using polymer resins with in situ product recovery (ISPR) applications. In: AIChE Annual meeting 2009, Paper 564f, Nashville
49. Woodley JM, Bisschops M, Straathof AJJ, Ottens M (2009) Future directions of in-situ product removal (ISPR). J Chem Technol Biotechnol 83(2):121–123
50. Klasson KT, Ackerson MD, Clausen EC, Gaday JL (1991) Bioreactor design for synthesis gas fermentations. Fuel 70(5):605–614
51. Clausen EC, Gaddy JL (2009) Ethanol from biomass by gasification/fermentation. http://www.anl.gov/PCS/acsfuel/preprint%20archive/Files/38_3_CHICAGO_08-93_0855.pdf. Accessed 20 April 2017
52. Bruce WF, President, The co-production of ethanol and electricity from carbon-based wastes, BRI Energy
53. Chen J, Gomez JA, Höffner K, Barton PI, Henson MA (2015) Metabolic modeling of synthesis gas fermentation in bubble column reactors. Biotechnol Biofuels 8(89):1–12
54. Vandecasteele J (2016) Experimental and modelling study of pure-culture syngas fermentation for biofuels production. MSc Universiteit Gent

55. Malmierca S, Díez-Antoínez R, Paniagua AI, Martín M (2017) Technoeconomic study of AB biobutanol production. Part 2: process design. Ind Eng Chem Res 56(6):1525–1533
56. Shinto H, Tashiro Y, Kobayashi G, Sekiguchi T, Hanai T, Kuriya Y, Okamoto M, Sonomoto K (2008) Kinetic study of substrate dependency for higher butanol production in acetone-butanol-ethanol fermentation. Process Biochem 43:1452–1461
57. Raganati F, Procentese A, Olivieri G, Götz P, Salatino P, Marzocchella A (2015) Kinetic study of butanol production from various sugars by *Clostridium acetobutylicum* using a dynamic model. Biochem Eng J 99:156–166